NARROW-BAND ELECTRONS IN TRANSITION-METAL OXIDES

JOHN B. GOODENOUGH

Lincoln Laboratory), Massachusetts Institute of Technology, Lexington**)*

Experiments on $LaCoO_3$ demonstrate that crystal-field theory and band theory describe two thermodynamically different electronic phases. For an integral number of electrons per atom, the phase transition is first-order. The critical parameter is an overlap integral, which may be either a cation–cation or a cation–anion–cation overlap integral. Intra-atomic exchange and electron–phonon interactions contribute significantly to electron localization. The characteristic feature of collective electrons is a Fermi surface. Those physical properties that depend upon the existence of a Fermi surface vary discontinuously through a localized-electron $\rightleftarrows$ collective-electron transition; other physical properties, including electron mobility and paramagnetic susceptibility, apparently do not. It is argued that the spontaneous crystallographic distortions associated with semiconducting $\rightleftarrows$ metallic phase changes manifest the existence of narrow, cation–sublattice bands if the cations are removed from the centers of symmetry of their interstices, narrow crystalline bands otherwise; ferroelectric and antiferroelectric transitions manifest the existence of a narrow valence band; the formation of a homologous series of shear structures in nonstoichiometric compounds manifests narrow conduction bands. These distortions all result from the creation, or enhancement, of an energy discontinuity at the Fermi surface. By contrast, conventional Jahn-Teller distortions, magnetostriction due to spin-orbit coupling, and the ordering of small polarons manifest localized electrons and the applicability of crystal-field theory. It is also shown that the critical overlap integral (or bandwidth) for spontaneous band magnetism is only a little larger than that for a localized-electron $\rightleftarrows$ collective-electron transition. Preliminary data are compatible with two possibilities for bands that are more than half-filled: (1) saturation of orbitals of α spin, which leads to localized electrons of α spin and collective electrons of β spin; (2) spontaneous magnetization (ferromagnetism) of only the antibonding electrons, which may lead to reduced atomic moments. Spontaneous band antiferromagnetism may be stabilized in bands that are half-filled or slightly less. It is represented by a spin-density wave with wavelength adjusted to create an energy discontinuity at the Fermi surface. Spin-density waves are also possible among collective β-spin electrons that are coupled to localized α-spin electrons.

I. INTRODUCTION

There are two limiting descriptions of the atomic outer electrons in solids: crystal-field theory and band theory. Crystal-field theory rests on the assumption that the outer electrons are localized to discrete atomic positions, whereas in band theory it is assumed that each electron is shared collectively by all of the atoms in a periodic array. Outer *s* and *p* electrons must usually be described by band theory. Only in special situations do they form narrow bands. Outer 4*f* electrons, on the other hand, are tightly bound to their atomic nuclei and are always described by crystal-field theory. The theory of transition-metal compounds is complicated because outer *d* electrons represent an intermediate case: In some crystals they can be described by

*) *Operated with support from the U.S. Air Force.*

**) *C-126 Lincoln Laboratory, Lexington 73, Massachusetts 02173, U.S.A.*

crystal-field theory, in others by a collective-electron model, and in a few both localized and collective d electrons appear to be present simultaneously.

Transition-metal oxides provide a particularly important illustration of the intermediate character of outer d electrons. There are three reasons why this is so: (1) The electronegativity difference between cations and anions is so large that the outer s and p orbitals form filled valence bands and empty conduction bands that are split by a large energy gap. This means that the electronic properties are imparted by the d electrons, which have energies that are within this gap. (2) There are several isostructural series within which different compounds exhibit d electrons of different character. Therefore they permit us to study the transition from a localized-electron to a collective-electron situation. (3) In oxides, the conditions for localized d electrons may be broken down either by cation–cation interactions or by cation–anion–cation interactions, or by both simultaneously. Thus transition-metal oxides permit us to study two types of narrow-band electrons: those that are confined to a cation sublattice and those that belong to the crystal as a whole.

II. PHYSICAL PROPERTIES DEPENDENT UPON LOCALIZED VS. BAND ELECTRONS

Before we can define a narrow-band charge carrier, it is necessary to ask whether a localized-electron model and a collective-electron model correspond to two different electronic phases, separated by a sharp phase boundary, or whether they are two limiting descriptions of the same electronic phase. This is a meaningful physical question, since the two models give quite different descriptions of several physical properties. If there is only one electronic phase, these properties should vary continuously from the collective-electron description to the localized-electron description. However, if there are two phases, then there will be a discontinuous transition in at least some of these properties, and we can expect to find some situations where localized and collective d electrons coexist. Some of the pertinent physical properties are summarized in Table 1.

Since a discontinuity in electron population vs. energy occurs at the Fermi energy at $T = 0°K$ in a partially filled band, properties that depend upon the existence of a Fermi surface can distinguish collective electrons from localized electrons.

In conventional one-electron band theory, there are two interactions that are either partially neglected or are treated only in perturbation theory: intraband electron–electron interactions and electron–phonon interactions. Since the magnitudes of these two interaction energies increase as the bandwidth narrows, they play an increasingly important role in the description of narrow-band electrons. In fact, if the bands are narrow enough, each of these interactions by itself may induce collective electrons to be transformed into localized electrons. Therefore properties that depend on these interactions are also listed in Table 1.

A. The Fermi Surface

The concept of a Fermi surface is particularly important if there are an integral number of d electrons per like transition-metal ion, because a localized-electron $\rightleftarrows$ $\rightleftarrows$ collective-electron transition to partially filled bands requires the creation of a Fermi surface at the Fermi energy. Consequently those physical properties that de-

Table 1

Properties of localized vs. collective electrons
(Two phases or twolimiting theories?)

Property	Localized	Collective
A. Fermi Energy Surface in Partially Filled Bands		
Definite Fermi Surface	No	Yes
Optical Reflectance	Limited	With sharp ω_p
Magnetic-spiral Wave Length	Exchange-dependent	E_F-dependent
Crystal Distortions	Local[a]	Translational
Nonstoichiometry	Point Defects	Shear Structures[b]
B. Electron–Electron Interactions		
Atomic Moment	"Atomic"[c]	Reduced[d] or None
Paramagnetic χ_m	Curie-Weiss	Pauli[e]
Magnetic Exchange	Short-range[f]	Long-range
Superconductivity	No	Possible
C. Electron-Phonon Interactions		
Polarons	Small	Large
Conductivity	Activated[g]	$n_{eff}e^2\tau/m^{*}$[h]
Seebeck Voltage Change[i]	$>100\ \mu V/°C$, Yes	$<20\ \mu V/°C$, Maybe[j]

[a] Local distortions may be cooperative.

[b] Compounds containing heavy ions with outer-electron configuration s^2, like Pb^{2+} and Bi^{3+}, may have isolated anion vacancies acting as electron traps for trap-mediated metal–metal bonds. (J. M. Longo, P. M. Raccah and J. B. Goodenough, to be published.)

[c] Crystalline fields may quench orbital contribution. Large crystalline fields ($\Delta_{cf} > \Delta_{ex}$) may stabilize low-spin state.

[d] If narrow bands more than three-quarters filled, spontaneous band ferromagnetism gives full "atomic" moment. Also, β-spin collective electrons in presence of localized α-spin electrons results in full "atomic" moment.

[e] Narrow-band electrons may give temperature-dependent paramagnetism, but effective Curie constant cannot be simply related to an atomic moment.

[f] Heisenberg exchange Hamiltonian if an integral number of d electrons per lik ecation; double-exchange Hamiltonian otherwise. Double-exchange Hamiltonian becomes long-range Hamiltonian if mobile electrons become collective.

[g] Activation energy in mobility for small-polaron conduction; activation energy in number of mobile carriers if conduction via electrons excited from small-polaron to collective-electron states.

[h] Activated if full band is separated from empty band by a finite energy gap.

[i] Maximum magnitude and change in sign of Seebeck voltage on changing composition through a stoichiometry corresponding to integral number of d electrons per like cation.

[j] Larger Seebeck voltages and change of sign are obtained if stoichiometry corresponds to a full band separated from an empty band by finite energy gap.

pend upon the existence of a Fermi surface appear abruptly at the transition. In addition, since the localized electrons are "frozen" at discrete atomic positions to form a "Fermi solid", whereas collective electrons form a "Fermi gas" moving in a periodic potential, we may anticipate that creation of a Fermi surface introduces a discontinuity in the electron entropy, which by definition means that the crystal-field and band models correspond to two thermodynamically different electronic phases that are separated by a first-order phase change. It follows that we may also anticipate a discontinuous change in at least those physical properties that depend upon the existence of a Fermi surface. There is no à priori reason why other physical properties should be discontinuous at a first-order, localized-electron $\rightleftarrows$ collective-electron transition, but we can expect them to at least vary rapidly on passing from one regime to the other.

Where there are a nonintegral number of d electrons per like transition-metal atom, i.e. the existence of two like atoms in two different valence states, the situation is less straightforward. Conceptually, it is necessary to use a band model, even if electron–phonon interactions are so strong that lattice relaxations have trapped the electrons at discrete atomic positions (small-polaron limit discussed in Paragraph D below). However, interactions between small polarons are short-range whereas those between collective electrons (or large polarons) are long-range. Since it is the long-range character of the collective electrons in a Fermi gas that is responsible for a discontinuity in the electron population at the Fermi surface, there is no well-defined Fermi surface in the small-polaron limit and the physical properties associated with a Fermi surface may only occur in the large-polaron regime. Since we may anticipate an abrupt, though not necessarily first-order, transition from short-range to long-range electron correlations, it is predicted that the small-polaron $\rightleftarrows$ large-polaron transition is sharply defined. Because small-polaron interactions are short-range, intra-atomic exchange dominates interatomic exchange and crystal-field theory is applicable in the small-polaron limit; small-polaron bands are extremely narrow. Therefore the crystal-field and band models should also correspond to two thermodynamically different electronic states in the case of a nonintegral number of d electrons per like transition-metal atom.

The fact that collective electrons in partially filled bands have a Fermi surface means that they may be distinguished from localized electrons by those properties that depend upon the existence of a Fermi surface. For example, collective electrons in partially filled bands exhibit a reflectance spectrum with a sharp cutoff at the plasma frequency ω_p. This reflectance is responsible for a characteristic metallic luster. The physical properties I will stress in this paper are the occurrences of long-range periodicities, either in magnetic order or in atomic order, that either introduce or enhance a surface of energy discontinuity at the Fermi surface in reciprocal space.

B. Spontaneous Crystallographic Distortions

1. *Localized electrons*: Crystallographic distortions due to localized electrons are characteristically local deformations, but if there are a large enough number of these local deformations to interact with one another, these deformations will be ordered so as to give a cooperative distortion of the crystal as a whole. There are two types of local deformations: ordering of electrons among degenerate localized orbitals that produces a less symmetric charge distribution, thus deforming the site to stabilize the order, and trapping of charge carriers at specific cationic sites via atomic deformations that create a unique potential at those sites. The first type is illustrated by Jahn-Teller distortions and by magnetostrictive distortions due to spin-orbit coupling [1]. The second type is illustrated by the formation of small polarons (Landau trapping) in compounds having the same atom in two different valence states. For the first type, cooperative distortions are achieved by ordering the unique axes of the asymmetric charge distribution so as to minimize the elastic energy. For the second, cooperative distortions are achieved by ordering the small polarons – and any associated lattice defects – so as to optimize the sum of the elastic and electrostatic energies. In low-temperature ($T < 119°K$) Fe_3O_4, for example, Fe^{2+} and Fe^{3+} ions are ordered on alternate (001) planes [2][1]); in $Fe_{1-x}O$, on the other hand, not onlyFe^{3+} and Fe^{2+} ions, but also the cationic vacancies order cooperatively [3]. Although these local distortions may thus be cooperative, introducing a macroscopic distortion of the crystal, nevertheless the cations always remain in the centers of symmetry of their anionic interstices, since localized orbitals are always centrosymmetric with respect to the cationic nucleus. (Displacements from the center of symmetry of the anion interstice as a result of asymmetric electrostatic forces, as in Al_2O_3, are a trivial exception.)

2. *Collective electrons*: The characteristic feature of collective electrons, on the other hand, is the existence of a Fermi surface. A change in the translational symmetry that creates, or increases, an energy discontinuity at the Fermi surface stabilizes the energies of the occupied orbitals and destabilizes the energies of the unoccupied orbitals. There are four classes of distortions in transition-metal oxides that appear to illustrate this general principle, of which the first three characteristically exhibit a displacement of the cations away from the centers of symmetry of their interstices: (1) semiconducting ⇄ metallic transitions due to changes in the translational symmetry of the cationic subarray, (2) ferroelectric or antiferroelectric distortions, (3) shear structures of a homologous series of non-stoichiometric compounds, and (4) semiconducting ⇄ metallic transitions due to changes in the translational symmetry of the cation-anion array.

Semiconducting ⇄ metallic transitions: In order to illustrate the type of displace-

[1]) It is possible that the transition at 119°K in Fe_3O_4 marks a localized-electron ⇄ collective-electron transition, the localized-electron state being stabilized by the electronic ordering.

ment that would introduce an energy discontinuity, or Brillouin-zone surface, at the Fermi surface, consider a linear chain of N evenly spaced atoms, each atom containing one electron in an atomic orbital that overlaps the comparable orbital on its two near neighbors. The band of collective-electron states is then half-filled, and the conductivity is metallic. This might correspond, for example, to high-temperature VO_2, which has the rutile structure, one outer d electron per cation, and overlapping $d_{\|}$ orbitals parallel to the tetragonal c-axis. (Complications [4] from overlapping π^* bands due to $d_{\perp}$ covalent bonding with anion p_{π} orbitals can be overlooked in the present argument.) If the distance between atoms is a, then the chain may be thought of as two interpenetrating linear chains having atoms spaced $2a$ apart. If these two subchains are each displaced toward the other a distance δ, so that every other spacing is $a - 2\delta$ and the rest are $a + 2\delta$, then the periodicity of the chain is doubled and the reciprocal-lattice vector k is reduced from $2\pi/a$ to $k = \pi/a$. This means that in the reciprocal space of Fig. 1, an energy discontinuity (Brillouin-zone surface) is created at the Fermi surface at $k = \pm\pi/2a$.

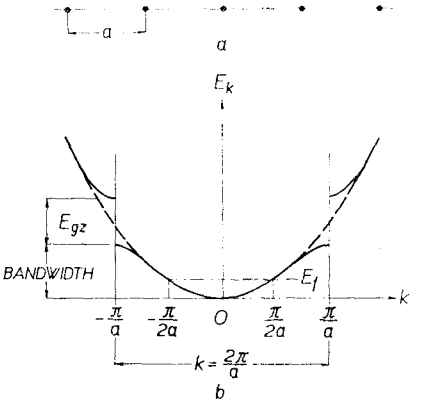

Fig. 1. Energy vs. wave vector for a linear chain of atoms having one overlapping orbital per atom. Fermi energy E_f corresponds to a half-filled band, or one electron per atom.

The magnitude of the energy gap E_{gz} across a Brillouin-zone surface depends upon the periodic potential. The potential at any point $\boldsymbol{r}$ in crystal space may be expanded as a Fourier series

$$U(\boldsymbol{r}) = \sum_{\boldsymbol{k}} U_{\boldsymbol{k}} \exp(i\boldsymbol{k} \cdot \boldsymbol{r}) \tag{1}$$

and for an energy discontinuity that is small relative to the bandwidth, Brillouin has shown that

$$E_{gz} = -2e|U_{\boldsymbol{k}}| = -2e\left|\sum_{t=1}^{s} A_{\boldsymbol{k}t} \exp(i\boldsymbol{k} \cdot \boldsymbol{n}_t)\right| \tag{2}$$

where $\boldsymbol{n}_t$ gives the positions in real space of the s atoms of the unit cell. If all the atoms are identical, then

$$U_{\boldsymbol{k}} = A_{\boldsymbol{k}} \sum_{t=1}^{s} \exp(i\boldsymbol{k} \cdot \boldsymbol{n}_t) = A_{\boldsymbol{k}} S_{\boldsymbol{k}} \tag{3}$$

where $S_{\boldsymbol{k}}$ is the usual structure factor of x-ray intensities. For the linear chain of paired atoms the new structure factor is

$$\begin{aligned} S_k &= \exp(i\pi\delta/a) + \exp(i\pi)\exp(-i\pi\delta/a) \\ &= 2i \sin(\pi\delta/a) \end{aligned} \tag{4}$$

which means that the energy discontinuity at the Fermi surface is

$$E_{gz} = A\delta + \ldots \tag{5}$$

Since the elastic restoring forces are proportional to δ^2, a spontaneous static distortion requires a stabilization of the occupied states that is linear in the displacements. Initially, where E_{gz} is small compared to the bandwidth $\Delta\varepsilon_b$, the number of states n_R that are stabilized is also proportional to δ, so that the total stabilization energy is

$$\Delta E = -\tfrac{1}{2}n_R E_{gz} = -A'\delta^2 + \ldots \tag{6}$$

and no spontaneous distortion is anticipated. This is why semiconducting $\rightleftarrows$ metallic transitions are not a general phenomenon in broad-band metals. However, if the bands are so narrow that $E_{gz} > \Delta\varepsilon_b$ for relatively small $\delta \geqq \delta_c$, then A' is large and $n_R \to N$ saturates for $\delta > \delta_c$. In this case

$$\Delta E = -A'\delta^2 \to -B\delta \quad \text{for} \quad \delta > \delta_c \tag{7}$$

and the conditions for a finite, spontaneous distortion are met. Further, note that for $E_{gz} > \Delta\varepsilon_b$ the width of the half-bands has been reduced to nearly zero: this corresponds to trapping the conducting electrons into homopolar, metal–metal bonds in the linkages of length $a - 2\delta$ along the chain.

In order to illustrate the problem in two dimensions, consider a close-packed planar net and a quarter-filled planar band corresponding to one electron per cation in the two orbitals

$$d_{\pm} = R_d(r)\{c_1\sqrt{2}\sin^2\Theta\exp(\mp 2i\varphi) \pm c_2\sin\Theta\cos\Theta\exp(\pm i\varphi)\} \tag{8}$$

that form Fe–Fe β-spin bands in the basal planes of hexagonal, high-temperature FeS [5]. Bertaut [6] has shown that, in the low-temperature phase, the cations form triangular clusters as shown in Fig. 2. This distorted configuration forms a hexagonal cell in the plane that is four times larger than the original cell, which introduces a Brillouin zone that is filled with one electron per atom. A similar distortion is anticipated for hexagonal $LiVO_2$, which has Li^+ and V^{3+} ions ordered on alternate (111) planes of the rocksalt structure, since the V–V bands contain two electrons per vanadium atom, which would just fill the second zone. As has been pointed out elsewhere [7], the triangular clusters in FeS are bound by three-electron bonds (two α-spin and one β-spin electron per Fe^{2+} ion); in $LiVO_2$ they are bound by two-electron bonds.

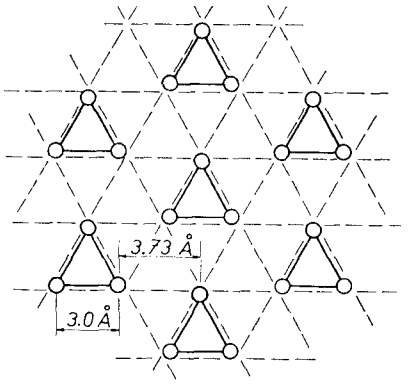

Fig. 2. Triangular cluster formation within (001) ion planes of low-temperature FeS.

More complicated cluster-formation is possible. For example, if there were 0·5 electrons per atom in a square net, the net might distort to form square clusters as shown in Fig. 3 in order to have a square Brillouin zone of edge π/a inside the original zone of side $2\pi/a$. With 0·8 electrons per atom, a square net might distort as shown in Fig. 4.

In all of these illustrations, we have restricted ourselves to collective-electron states that have been formed by the overlap of atomic orbitals on near-neighbor transition-metal ions. Such states will be referred to as cation-sublattice band states. Spontaneous distortions that transform narrow-band cation-sublattice states into "cluster" states, as just described, exhibit two characteristic properties: they occur at a first-order semiconducting $\rightleftarrows$ metallic phase transition and the cations are moved out of the centers of symmetry of their anion interstices toward one another. (However, it is possible to have a transition temperature $T_t \geqq T_{mp}$, where T_{mp} is the melting point.) The transition is first-order because the stabilization achieved by the distortion

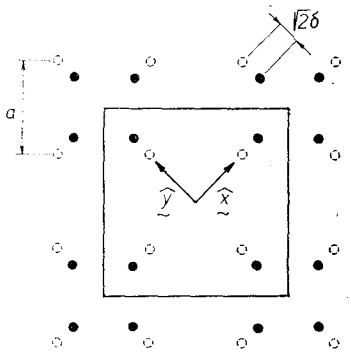

Fig. 3. Theoretical cluster formation for a planar phonon array having narrow bands one-quarter filled.

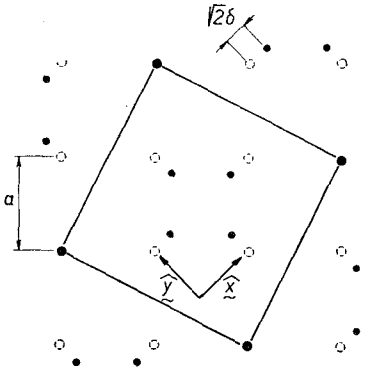

Fig. 4. Theoretical cluster formation for a square planar array having narrow bands four-fifths filled.

is reduced by thermal excitation of n of the stabilized electrons across $E_g = fE_{gz}$, $0 < f \leqq 1$, into the states that are destabilized by the distortion. The change in internal energy due to the displacements has the form

$$\Delta E = -A\delta + \tfrac{1}{2}B\delta^2 = [A_0 - n(E_g/a)]\,\delta + \tfrac{1}{2}B\delta^2 \tag{9}$$

The displacement that optimizes ΔE is

$$\delta = \delta_0 - n(E_g/aB) \tag{10}$$

where δ_0 is the displacement at $T = 0°\mathrm{K}$. Therefore, to first order in δ, the energy gap E_g is

$$\tfrac{1}{2}E_g = |A\delta| = A_0\delta_0 - E_g(2n\delta_0/a) \approx \tfrac{1}{2}E_{g0}(1 - 2n\delta_0/a) \tag{11}$$

$$n = n_0 \exp(-E_g/2kT) = n_0 \exp(nE_{g0}\delta_0/akT) \exp(-E_{g0}/2kT) \tag{12}$$

which leads to a catastrophic increase in n at a finite temperature [8].

If a crystalline band (band formation of d electrons due to covalent mixing with anion orbitals, as described in Section III) is half-filled, spontaneous distortions that change the translational symmetry may not remove the cations from the center of symmetry of their anion interstices. Compare, for example, NiO with PdO and PtO. In NiO the nickel d electrons are localized, and the orbital degeneracy associated with two d holes per Ni^{2+} ion is removed by intra-atomic exchange splitting of orbitals of α spin from those of β spin. In PdO and PtO, on the other hand, there is considerable covalent mixing of anionic orbitals with the cationic orbitals that σ bond with the anions, and the d holes occupy collective-electron states. If the structure were rocksalt, as in NiO, the narrow bands of collective-electron states (twofold-degenerate e_g bands) would be half-filled and intraband exchange interactions could only introduce a relatively small stabilization associated with a spin-density wave propagating along a [111] axis so as to introduce antiferromagnetic coupling between small ($\ll 1\mu_B$) atomic moments. Greater stabilization is achieved by a distortion to tetragonal symmetry having two molecules per primitive unit cell. This removes the twofold band degeneracy, making the compounds semiconductors rather than metals. This distortion is achieved without removing the cations from the centers of symmetry of their anionic interstices because of the band degeneracy. As pointed out by Pauling [9], this structure is due to considerable covalence, but from our point of view this covalence creates partially filled, collective-electron orbitals within a narrow energy band, and the distortion is a manifestation of this narrow-band formation.

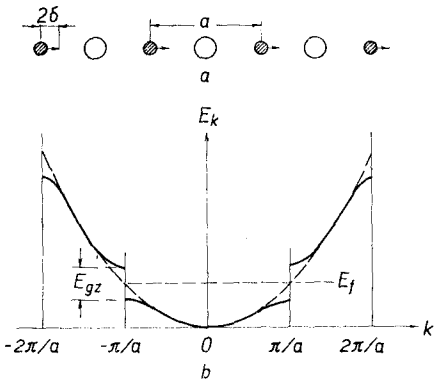

Fig. 5. Energy vs. wave vector for a linear chain of alternating anions and cations having one overlapping orbital per atom. Fermi energy E_f corresponds to a half-filled band, or one electron per atom.

Ferroelectric transitions: Ferroelectric or antiferroelectric transitions represent spontaneous distortions that increase the band gap between two narrow bands. Consider, for example, a linear chain of N atoms consisting of alternating cations and anions as shown in Fig. 5. To make contact with a physical situation (application to oxides with perovskite structure becomes apparent in Section VB), consider only the two anion p_π orbitals, p_x and p_y, and the two cation d orbitals that π-bond with these, d_{zx} and d_{yz}. Because of the difference in potential at the cations and the anions, the collective-electron π-bond orbitals have energies that are split into two bands, a π band of bonding orbitals that are primarily anionic in character and a π^* band of antibonding orbitals that are primarily cationic in character. With two electrons per atom (four electrons per cation-anion molecule), the π band is filled and the π^* band is empty. From Eq. (2), the energy gap between the π and π^* bands is

$$E_{gz} = -2e|A_M - A_0| \tag{13}$$

where A_M and A_0 are the A_k for the cation and anion, respectively. If the two sublattices are displaced toward one another a distance δ, then this energy increases:

$$E_{gz} = -2e\{|A_M + A_0| + (A_M + A_0)\, q\delta + \ldots\}\,. \tag{14}$$

Therefore if the two bands are so narrow that the number of states that are stabilized by the distortion is $n_R \to 2N$ for small δ, then a finite, spontaneous distortion will occur at lower T. Further, such a distortion will tend to localize the π-band electrons into cation–anion molecular-cluster orbitals. Note also that if n additional electrons are introduced, the stabilization energy is reduced as in Eq. (9), and the transition temperature T_t is reduced or the distorted phase completely suppressed.

Shear structures: Several nonstoichiometric oxide systems have been shown to consist of a homologous series of discrete phases rather of a broad range of solid solubility with randomly distributed defects. Magnéli and his co-workers have identified, for exaple, the series Ti_nO_{2n-1} [10], $(W, M)_nO_{3n-2}$ with $M = Nb$ or Ta [11], and $(W, Mo)_nO_{3n-1}$ [12]. These homologous series are to be distinguished from other ordered-defect phases, such as are found in PrO_{2-x} [13] or $Fe_{1-x}O$ [3], by the characteristic occurrence of crystal shear at regularly spaced intervals. The other compounds, which contain localized d or f electrons, are characterized by ordered point defects. Since the systems that exhibit homologous series all appear to contain collective d electrons, whereas those with ordered point defects appear to contain localized d or f electrons, it suggests that the surprising regularity of the spacings between shear planes is due to the existence of a Fermi surface and the energy stabilization to be achieved by either creating or increasing the energy discontinuity across a Brillouin zone at the Fermi surface. Magnéli [14] has already pointed out how condensation of the defects into common planes minimizes the elastic energy of the crystal, but this does not explain why these planes are regularly spaced. However, it does show that any stabilization due to the creation of a new periodicity via regular spacing of the planes only has to be greter than the entropic energy at temperatures high enough for diffusion to occur. This stabilization is greater the narrover the bands, just as for the semi-conducting $\rightleftarrows$ metallic transitions and the ferroelectric transitions.

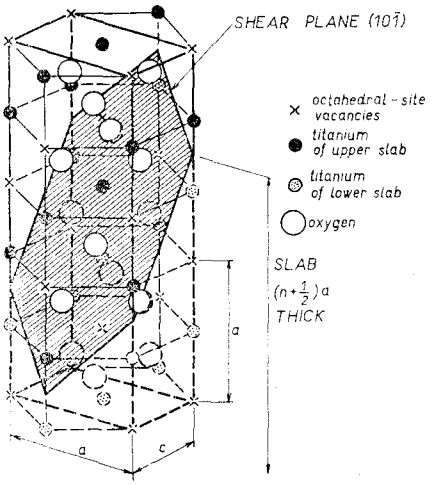

Fig. 6. Shear plane in Ti_nO_{2n-1} structure; c, a, (10$\bar{1}$) refer to axes of rutile slabs.

To illustrate this concept, consider Ti_nO_{2n-1}, which has rutile slabs n titanium atoms thick that are connected by shear planes across which the titanium octahedra share common faces, as shown in Fig. 6. These shear planes are so spaced that if the titanium ions are given formal charges $+3$ and $+4$, all of the Ti^{3+} ions could face one another across the shared octahedral-site faces. However, with the exception of low-temperature Ti_3O_5, the Ti–Ti spacing across these faces is relatively large, indicating that Ti^{3+}–Ti^{3+} homopolar bonding across the shear planes

ductor $\rightleftarrows$ metallic transition is not competitive with a ferroelectric-type transition, which displaces the cations away from each other across the shear planes. Displacements of the cations towards one another would reduce the electrostatic repulsion across a shared face by concentrating electronic charge in homopolar Ti^{3+}–Ti^{3+} bonds. Displacements away from one another reduce the electrostatic repulsion by increasing both the cation–cation separation and the anionic shielding. In either mode, the effect is enhanced by a periodic spacing, since this concentrates cooperatively the influence of the distortions to a definite group of collective-electron orbitals, does not take place at room temperature. This means that at high temperatures the semiconstabilizing some at the expense of others. (Localized orbitals would have only a short-range influence.) Since the energy gap between those occupied and unoccupied orbitals influenced by the transition is larger for the ferroelectric mode, this mode dominates at high temperatures where the periodic structures are initially formed.

It is interesting to note that all of these manifestations of the Fermi surface, like that of stabilization of the wave length of a spin-density wave [15], are more prominant the narrower the band. This makes them particularly useful for distinguishing narrow-band orbitals from localized orbitals. By contrast, long-range ordering of antiphase domain boundaries in alloys [16] does not reguire narrow bands.

C. Electron-Electron Interactions: Magnetism

Electron-electron interactions are responsible for spontaneous magnetic properties (See Table 1). In the case of localized electrons, intra-atomic exchange forces split

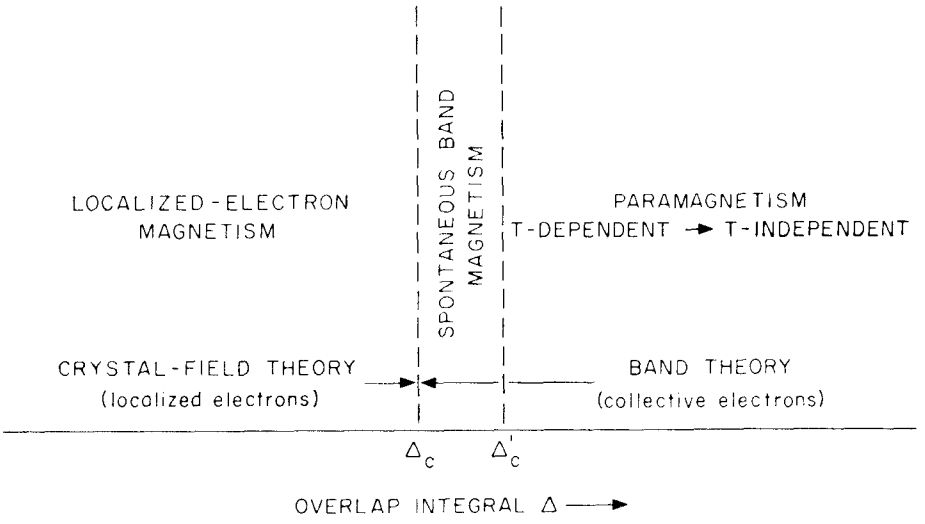

Fig. 7. Variations in magnetic properties as a function of the overlap integrals.

the orbitals of different spin (unless crystal-field splittings are too large), just as in the free atom. This produces a spontaneous, localized atomic moment and a paramagnetic susceptibility that obeys a Curie-Weiss law (unless multiplet splittings are $\sim kT$).

The interatomic exchange forces responsible for long-range magnetic order are themselves short-range and well described by superexchange and double-exchange theory. Collective electrons, on the other hand, usually exhibit a weak, temperature-independent magnetic susceptibility (diamagnetism or Pauli paramagnetism).

One of the important questions for the theory of magnetism is whether the critical bandwidth for localized vs. collective electrons is larger or smaller than the critical bandwidth for spontaneous band magnetism. If it is larger, spontaneous band magnetism will only be found where localized-electron atomic moments are simultaneously present. If it is smaller, as indicated schematically in Fig. 7, there will be a narrow range of bandwidths for which spontaneous band magnetism occurs, and this range acts as a bridge between localized-electron magnetism and temperature-independent Pauli paramagnetism. It is important to find materials that have bandwidths within this limited range so that the properties of spontaneous band magnetism may be studied as a function of bandwidth and band population and compared with the properties of localized-electron magnetism. Two distinguishing features of collective-electron antiferromagnetism vs. localized-electron antiferromagnetism are (1) a reduced atomic moment and (2) a spin-density-wave periodicity that creates an energy discontinuity at the Fermi surface. Antiferromagnetic, spiral spin configurations for localized-electron atomic moments have a periodicity that is determined by the magnitudes of competitive short-range interactions [17–19].

D. Electron-Phonon Interactions: Transport Properties

1. *Definition of the polaron*: If the number of conduction electrons is a very small fraction of the number of atoms, electron–electron interactions are relatively unimportant and only electron–phonon interactions are a problem. Improvement of conventional band theory requires the introduction of atomic vibrations into the zero-order Hamiltonian. If this is done, a single collective electron becomes confined to a finite region of the crystal by cooperative atomic displacements that trap it, and the charge carrier consists of both the electron and its associated atomic displacements [20]. If the volume to which the collective electron is confined is large compared to an atomic volume, the charge carrier is called a large polaron. The localized-electron limit corresponds to such strong electron–phonon interactions that the polaron volume has shrunk to the volume of a single atom and its nearest neighbors. This is called a small polaron. (Refer to Table 1.)

2. *Electrical conductivity*: The electrical conductivity for a two-carrier (holes and electrons) situation is

$$\sigma = \sigma_- + \sigma_+ = ne\mu_n + pe\mu_p \tag{15}$$

where e is the charge of an electron, μ_n and μ_p are the mobilities, n and p are the numbers of electrons and holes per cm^3. In the small-polaron limit, a localized electron carries its local deformation with it, so that its speed is restricted to the speed of

sound, and it moves by hopping from one atomic position to a neighboring one by hopping over the elastic energy barrier associated with the motion of the deformation. Therefore its mobility is described by diffusion theory and contains an activation energy:

$$\mu_{\text{loc}} = (eD_0/kT) \exp(-\varepsilon_a/kT) . \tag{16}$$

An alternative mechanism is for a charge carrier to be thermally excited out of the low-mobility small-polaron state into a higher-mobility large-polaron state, only to become trapped again into a small-polaron state after travelling beyond its near neighbors for a mean-free time τ. In this case, the charge-carrier mobility has the same form as for collective electrons:

$$\mu_{\text{coll}} = e\tau/m^* \tag{17}$$

where m^* is the effective mass. However, the number of such higher-mobility charge carriers is

$$n_m = n \exp(-f\varepsilon_p/kT) \quad \text{or} \quad p_m = p \exp(-f\varepsilon_P/kT) \tag{18}$$

where ε_P is the energy difference between the narrow, small-polaron band and the bottom of the collective-electron band and $\frac{1}{2} < f < 1$ depends upon the number of charge carriers. If the small polarons are trapped at lattice defects[2]), or if $\varepsilon_a > \varepsilon_P$ for some other reason, the second mechanism will provide the dominant conduction mechanism. Nevertheless, the conductivity will contain an activation energy, even if the mobility does not, wherever the electrons are localized. On the other hand, the number n_{eff} of collective electrons or large polarons in a partially filled band is essentially constant and their mobilities have the form of Eq. (17). Therefore collective electrons in partially filled bands ($n = n_{eff}$ and $p = 0$ or $p = p_{eff}$ and $n = 0$) have no activation energy in the conductivity. If the conductivity increases logarithmically with the temperature, I shall refer to it as "semiconducting"; if it decreases with increasing temperature, I shall call it "metallic". Compounds having localized charge carriers or small polarons must be semiconducting.

Attempts have been made to construct a continuous theory from the large-polaron limit to the small-polaron limit. The essential physical idea has been that the polaron

---

[2]) In practice, the nonintegral number of d electrons is usually the result of either foreign atoms, as in $Li_xNi_{1-x}O$, or of ionic vacancies or interstitials, as in $Fe_{1-x}O$ or TiO_{2-x}. (Magnetite Fe_3O_4 is an interesting exception. See remark [1]) on page 308. These lattice irregularities create perturbations that are larger than the width of the band of small-polaron energies (or of narrow bands of large-polaron energies), and they trap the odd electrons or holes at donor or acceptor sites. If the number of trap sites is large enough for interactions between them, they tend to order and thereby deepen the traps. In this situation, the Fermi energy lies between the trap energies and the collective-electron energies, and electrons or holes only become charge carriers by excitation into the collective-electron bands.

volume should decrease continuously to the small-polaron limit as the magnitude of the electron–phonon interaction increases relative to the bandwidth. Holstein [21], for example, has predicted that the large-polaron band-width should decrease logarithmically with increasing temperature to give a sharp metallic ⇄ semiconducting transition with rising temperature. No one has yet observed such a transition. One difficulty with such a theory is that it fails to consider the intermediate mechanism discussed above. Above the transition temperature, $kT > \varepsilon_P$ can be anticipated, and the number of mobile charge carriers is saturated. Therefore electrical conductivity, which is independent of a Fermi surface, may not change abruptly through a localized-electron ⇄ collective-electron transition.

3. *Seebeck Voltage*: The Seebeck voltage for localized holes and electrons (small polarons) is [22]

$$\alpha\,(\text{intrinsic}) = (\alpha_+\sigma_+ + \alpha_-\sigma_-)/(\sigma_- + \sigma_+) \tag{19}$$

$$\alpha_\pm\,(\text{extrinsic}) = \pm(k/e)\,\{S^*/k + \ln\,[(1 - c_\pm)/c_\pm]\} \tag{20}$$

where S^* is the thermal contribution to the entropy that is transported by the charge carriers and $c_\pm \leqq \frac{1}{2}$ is the cationic ratio at $T = 0°\text{K}$

$$c_+ = M^{(m+1)}/(M^{m+} + M^{(m+1)+}) \quad \text{or} \quad c_- = M^{(m-1)+}/(M^{m+} + M^{(m-1)+}) \tag{21}$$

which gives the number of small polarons per transition-metal ion M at $T = 0°\text{K}$. In the limiting, intrinsic case $c_+ = c_- = 0$, the number of charge carriers is [22]

$$n = p = n_0 \exp\,(-\varepsilon_g/2kT) \tag{22}$$

where ε_g is the energy required to create a separated hole-electron, small-polaron pair $M^{(m+1)+}$ and $M^{(m-1)+}$. This energy goes to zero as the conditions for transformation from localized to collective electrons are approached. Therefore for a finite temperature the range of c over which the transport properties are intrinsic increases from a narrow interval to a large interval and the distinction between intrinsic and extrinsic properties disappears as the collective-electron regime is approached from the localized-electron limit.

In the small-polaron limit, α (extrinsic) achieves large numerical values ($|\alpha| > 100\ \mu\text{V/deg}$) as c_+ or c_- approaches zero, since the intrinsic domain is not reached until c is small, and there is an abrupt change of sign as the chemistry is varied through $c_+ = c_- = 0$ [23]. However, this sharp transition washes out as $\varepsilon_g \to 0$, and $|\alpha| = |\alpha\,(\text{intrinsic})| < 20\ \mu\text{V/deg}$. Again there is no dependence on the existence of a Fermi surface, so that there is no reason to require an abrupt change in the Seebeck voltage on passing through a localized-electron ⇄ collective-electron transition.

III. CRITICAL OVERLAP INTEGRAL FOR LOCALIZED VS. COLLECTIVE ELECTRONS

Before we compare the physical properties of isostructural transition-metal oxides, we must first consider how the localized-electron assumption of crystal-field theory is broken down. Let Fig. 8 represent a (100) plane of the rocksalt structure. By symmetry, the five d orbitals of an octahedral-site cation are split by the crystalline fields into two groups: a twofold-degenerate group of e_g symmetry, which is directed toward near-neighbor anions and is outlined by a solid line, and a threefold-degenerate group of t_{2g} symmetry, which is directed toward near-neighbor cations and is outlined by a dashed line. Note that covalent mixing of cationic d and anionic s and p orbitals does not destroy this symmetry classification. The orbitals of e_g symmetry are orthogonal to the anionic p_π orbitals and therefore are only modified by covalent mixing with the anionic s and p_σ orbitals. Orbitals of t_{2g} symmetry, on the other hand, are orthogonal to the anionic s and p_σ orbitals and are only modified by covalent mixing with cationic orbitals and the anionic p_π orbitals. We shall designate the covalent-mixing parameters λ_σ and λ_π, respectively. They are defined in terms of the crystal-field wave functions of e_g and t_{2g} symmetry:

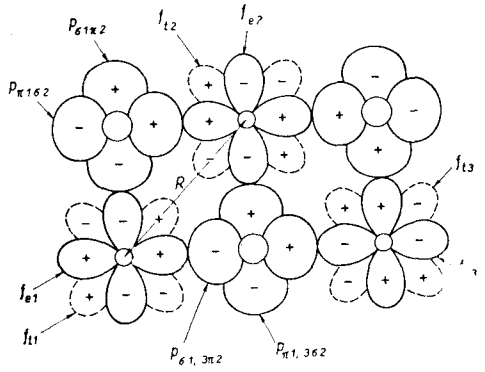

Fig. 8. Schematic representation of transition-metal cations and anions in (100) plane of a rock-salt crystal showing cationic orbitals of t_{2g} and e_g symmetry and anionic p orbitals.

$$\Psi_e = N_\sigma(f_e + \lambda_\sigma\varphi_\sigma) \tag{23}$$

and $$\Psi_t = N_\pi(f_t + \lambda_\pi\varphi_\pi + \lambda_c\varphi_c)$$

where f_e and f_t are the corresponding atomic orbitals, N_σ and N_π are normalization constants, and $\varphi_\sigma, \varphi_\pi, \varphi_c$ contain the anionic or near-neighbor-cationic s and p orbitals that are admixed via covalence.

Now, whether the d electrons are localized or collective depends upon the magnitude of the overlap integrals for d orbitals on neighboring cations. There are two types of integrals that can occur: (1) cation-cation overlap of t_{2g} orbitals

$$\Delta_{cc} \equiv |(\Psi_{t1}, \Psi_{t2})| = N_\pi^2[f_{t1}, f_{t2}) + \lambda\{(\varphi_{c1}, \varphi_{c2})], \tag{24}$$

and (2) cation-anion-cation overlap of either e_g orbitals on opposite sides of an anion

$$\Delta^\sigma_{cac} \equiv |(\Psi_{e1}, \Psi_{e3})| = N_\sigma^2\lambda_\sigma^2, \tag{25}$$

of t_{2g} orbitals on opposite sides of an anion

$$\Delta^\pi_{cac} \equiv |(\Psi_{t1}, \Psi_{t3})| = N_\pi^2[\lambda_\pi^2 + \lambda_c^2 + 2\lambda_\pi(f_t, \varphi_\pi) + 2\lambda_c(f_t, \varphi_c)] \tag{26}$$

or of a t_{2g} orbital with an e_g orbital of a near-neighbor cation via an anion p orbital that π bonds with one cation and σ bonds with the other,

$$\Delta_{cac}^{\pi\sigma} \equiv |(\Psi_{t1}, \Psi_{e2})| = N_\pi N_\sigma [\lambda_\pi \lambda_\sigma + \lambda_\sigma \lambda_c (\varphi_\sigma, \varphi_c)] . \tag{27}$$

What we are looking for, then, is a critical overlap integral Δ_c such that the d electrons are localized if $\Delta < \Delta_c$ and are collective if $\Delta > \Delta_c$. If Δ_c is sharply defined, it will indicate that the crystal-field and band descriptions correspond to two different electronic phases.

IV. A CRITICAL CATION–CATION SEPARATION R_c

The magnitude of the cation–cation overlap integral Δ_{cc} varies sensitively with R. Therefore where cation–anion–cation interactions can be assumed small, it is meaningful to look for a critical separation R_c.

Table 2

Some Physical Properties of Monoxides of First Transition Series

	Structure	R (Å)	R_c (Å)[a]	Transport	Magnetic
TiO	B1, 15% Vac.	2·94	3·02	Metal	Pauli
VO	B1, 15% Vac.	2·89	2·92	s. c. ⇄ Metal	Weakly T-dependent, 117°K
CrO	Unstable	—	2·80	—	—
MnO	B1	3·14	2·66	s. c.	C–W, $\mu_s = 5\mu_B$, 122°K
FeO	B1	3·03	2·95	s. c.	C–W, $\mu_{s\parallel} = 3{\cdot}3\mu_B$, 198°K
CoO	B1	3·01	2·87	s. c.	C–W, $\mu_s \approx 3{\cdot}8\mu_B$, 291°K
NiO	B1	2·95	2·77	s. c.	C–W, $\mu_s = 2{\cdot}0\mu_B$, 440°K
CuO	Monocl.	2·89	2·65	s. c.	C–W, $\mu_s \approx 0{\cdot}6\mu_B$, 230°K

[a] $R_c^{3d}(M^{m+}\text{-oxides}) = \{3{\cdot}20 - 0{\cdot}05m - 0{\cdot}03(Z - Z_{Ti}) - 0{\cdot}04S_i(S_i + 1)\}$ Å.

Pertinent physical properties of the first-series monoxides are summarized in Table 2. Clearly TiO, which is superconducting below 1·5°K, has collective 3d electrons. Whether this is due to cation–cation overlap having an $R < R_c$ or to a 90° cation–anion–cation interaction ($\Delta_{cc} > \Delta_c$ or $\Delta_{cac}^{\pi\sigma} > \Delta_c$), or to both simultaneously, is not known unambiguously. However, the fact that VO exhibits a semiconducting ⇄ ⇄ metallic transition characteristic of a narrow cation-sublattice band indicates that $R < R_c$ in both compounds. The other compounds in this table are successfully described by crystal-field theory and superexchange, indicating that $R > R_c$ and that the cation–anion–cation overlap integrals are also all $\Delta_{cac} < \Delta_c$. The column R_c shows the values for R_c obtained from the empirical formula

$$R_c^{3d}(M^{m+}\text{-oxides}) = \{3{\cdot}20 - 0{\cdot}05m - 0{\cdot}03(Z - Z_{Ti}) - 0{\cdot}04S_i(S_i + 1\} \text{ Å} \tag{28}$$

and you see that we change from $R < R_c$ to $R > R_c$ between VO and MnO. The second and third terms in this formula reflect the contraction of the $3d$ orbitals with increasing "effective" nuclear charge – here m is the formal cationic charge and Z is the atomic number – and the last term reflects the contraction due to intra-atomic exchange. Coefficients have been chosen to provide consistency with the data for this and similar systems containing 3+ and 4+ cations.

Although this type of data is compatible with the concept of a sharply defined R_c, we have not yet been able to find a chemical system that can demonstrate just how sharp R_c is. An alternative approach is to look for a critical cation–anion–cation overlap integral.

V. COMPOUNDS WITH THE ReO_3 AND PEROVSKITE STRUCTURE

A. Construction of Energy Diagrams

The ReO_3 and the perovskite structures form another important family of compounds. The ReO_3 structure of Fig. 9 consists of a simple-cubic cation sublattice with anions at the centers of the cube edges. In the cubic perovskite structure, with chemical formula ABO_3, the body-center position is occupied by a large A cation, and in the tungsten bronzes, Na_xWO_3, the body-center position is occupied randomly by the x

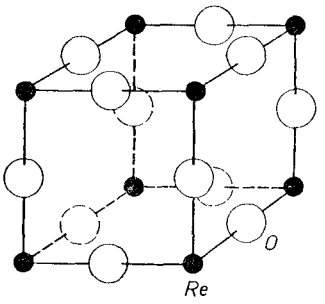

Fig. 9. The cubic ReO_3 structure.

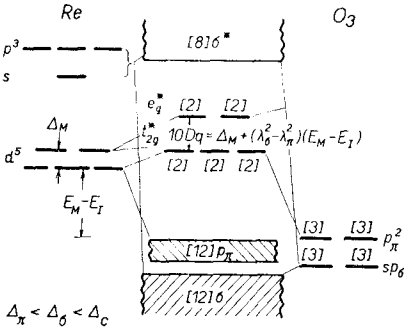

Fig. 10. Schematic, one-electron energies for localized d electrons in the ReO_3 structure.

sodium atoms. In the experiments under discussion here, this large ion has no outer d or f electrons and is strongly electropositive relative to the BO_3 array. It essentially acts as an electron donor to the bands of the BO_3 array.

Now note that the transition-metal B cations are separated across a cube edge by an anion intermediary and across a cube face by ~5·5 Å. From our empirical estimates of R_c, cation–cation interactions across the cube face can be assumed small, so that these structures provide an opportunity to study the transition from localized to collective d electrons with increasing cation–anion–cation overlap integrals.

In order to construct one-electron energy diagrams for the BO_3 array, note that

the B cations are in octahedral interstices and that the oxygen ions have only two near-neighbor cations, which are on opposite sides. The crystal fields split the anionic s and p orbitals into a twofold-degenerate pair of p_π orbitals and a more stable pair of hybridized sp_σ orbitals. These are shown in the right-hand column of Fig. 10. With three anions per formula unit, each of these orbitals is weighted by a factor three. They are stabilized relative to the cationic orbitals, shown in the left-hand column, by the electronegativity difference between the ions. The cationic $e_g^2 sp^3$ orbitals σ-bond with the six anionic sp_σ orbitals, and the three t_{2g} orbitals π-bond with three of the six anionic p_π orbitals. The outer s and p orbitals perturb one another strongly, giving rise to filled valence bands π and σ that are separated from an empty conduction band σ^* by a large energy gap.

There are three possibilities for the cationic d electrons. The first, shown here, corresponds to small covalent mixing of anionic orbitals into the five d orbitals. Note that π bonding is weaker than σ bonding, so that covalent mixing destabilizes the e_g orbitals more than the t_{2g} orbitals. This difference is responsible for the major contribution to the total crystal-field splitting $10Dq$.

If there is more than one outer d electron per cation, we must introduce a correction due to electron–electron interactions. The largest correction is the intra-atomic exchange, or Hund's rule splitting of different spin states, which is shown in Fig. 11.

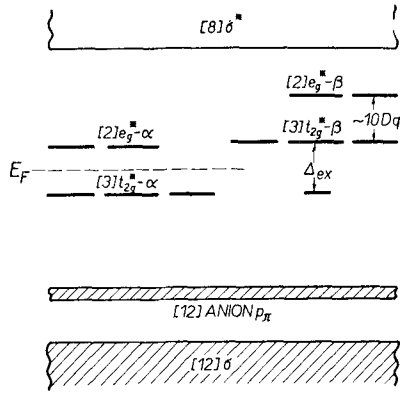

Fig. 11. Schematic, one-electron energies for more than one localized d electron in the ReO_3 structure.

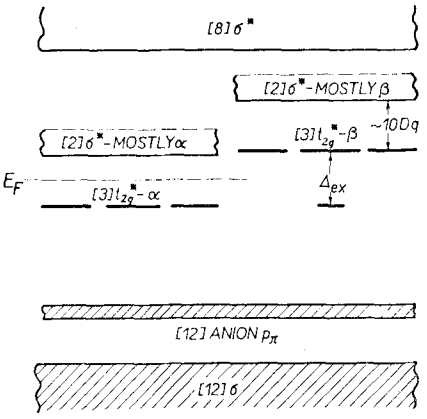

Fig. 12. Schematic one-electron energies for more than one t_{2g}^* electron per molecule in ReO_3 structure and $\Delta_{cac}^{\pi} < \Delta_c < \Delta_{cac}^{\sigma}$.

With more than one outer electron or hole, the spectroscopist uses multielectron energy levels, which are not to be confused with this one-electron diagram. We use the one-electron scheme in order to make contact with the conventional one-electron diagrams for collective-electron states.

If the π-band overlap integrals remain $\Delta_{cac}^{\pi} < \Delta_c$, but the σ-band overlap integrals become $\Delta_{cac}^{\sigma} > \Delta_c$, then the t_{2g} orbitals remain localized, but the e_g orbitals become transformed into band orbitals, as shown in Fig. 12. If the localized t_{2g} electrons have unpaired spins, Hund's splitting occurs just as in the previous case. If only t_{2g} electrons are present, all the d electrons are localized, and crystal-field theory can be used. The Fermi level shown here would correspond, for example, to a Cr^{3+} ion.

Finally, if both overlap integrals are greater than Δ_c, then the t_{2g} orbitals are also transformed into collective-electron states, as shown in Fig. 13.

These qualitative energy-level schemes apply to the perovskite structure as well as the ReO_3 structure, since the central A cation essentially acts as a donor to the BO_3 array.

B. Application: General Survey

We now ask whether there are any transition-metal oxides with the ReO_3 or perovskite structure that manifest collective d electrons. The first materials that come to mind are the sodium-tungsten bronzes Na_xWO_3. Here the WO_3 array is like ReO_3, and $x < 1$ sodium atoms per molecule are distributed randomly over the body-center sites. Cubic WO_3 would have no outer d electrons associated with the

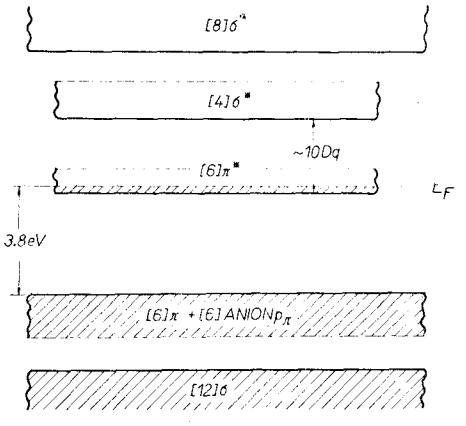

Fig. 13. Schematic one-electron energies for ReO_3 which has $\Delta_c < \Delta_{cac}^{\pi} < \Delta_{cac}^{\sigma}$.

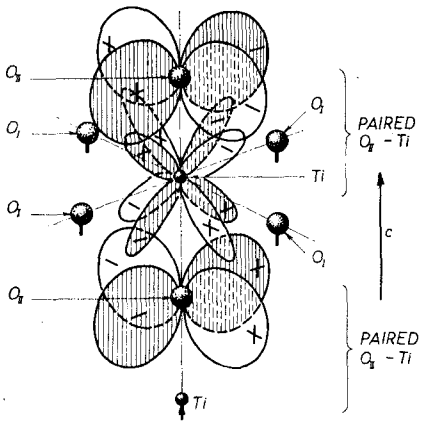

Fig. 14. Titanium ion shift from center of symmetry of anion interstice in tetragonal $BaTiO_3$ and the π-bonding orbitals primarily responsible for the reduced symmetry.

W^{6+} ions, and the Fermi energy would lie in the gap between the π and π^* bands. In the bronzes, the x Na atoms contribute x electrons to the π^* band, and the compounds are metallic and Pauli paramagnetic [24].

In order to be sure that π^*-band formation occurs and that there is no need to invoke a Na–Na band that overlaps the d levels, we decided to investigate the cubic compound ReO_3, which has

one outer *d* electron per molecule and no large A cations. According to the model given, it should contain one electron per molecule in the π^* band. Ferretti and Rogers [25] succeeded in preparing a reasonably stoichiometric single crystal of ReO_3. It is red with a metallic luster, it is diamagnetic, and it has a metallic conductivity nearly comparable to that of copper. Since there are no A cations in ReO_3, A-cation banding cannot account for the metallic character of this compound, and by Occam's razor, there is no need to involve it for the tungsten bronzes. Optical studies by Feinleib [26] have demonstrated a sharp reflectance cutoff, or a well-defined plasma frequency, and have provided the energy splitting shown in the slide.

In retrospect, it is not surprising that third-transition-series cations with formal valence 6+ have sufficient covalence for π^*-band formation. However, once it is realized that some oxides with perovskite structure are metallic while others, like $LaFeO_3$, are magnetic insulators, then it is clear that this structure permits a study of the change in properties from the localized-electron limit to the collective-electron limit as a result of changes in the magnitudes of the cation–anion–cation overlap integrals. Some simple perovskites that have been studied thus far are listed in Table 3. The compounds are arranged so that the rows correspond to a particular outer *d* shell and a given formal cationic charge. The columns correspond to the net potential spin for localized electrons. Compounds so designated contain low-spin cations. In region I of this diagram, all of the compounds have only collective *d* electrons, and in region III only localized *d* electrons. In region II the t_{2g} electrons are localized, but the e_g electrons are collective. The fact that region III is restricted to the high-spin ions clearly emphasizes the importance of intra-atomic exchange in stabilizing the localized-electron state.

Table 3

Localized vs. collective *d* electrons in transition-metal oxides with perovskite or ReO_3 structure

t^0e^0	t^1e^0	t^2e^0	t^4e^0	t^3e^0	t^3e^1	t^3e^2	$t^4e^2 + t^6e^0$	t^6e^1
$S = 0$	1/2	1	$(\frac{3}{2}\alpha - \frac{1}{2}\beta) = 1$	3/2	2	5/2	2 + 0	1/2

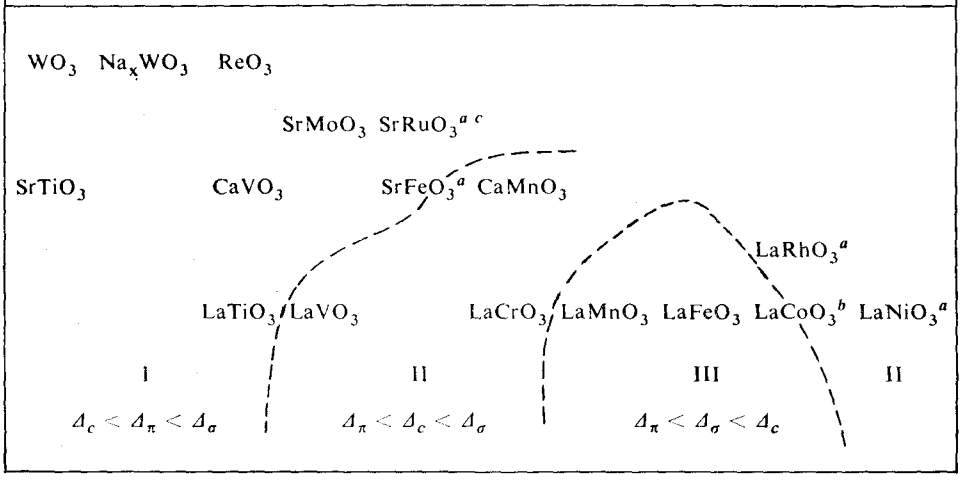

[a] Low-spin B cation.
[b] Low-spin Co^{3+} at 0°K, both high- and low-spin states at finite *T*.
[c] Ferromagnetic $\mu_0 = 0.8\mu_B$, or $S = 0.4$.

Frederickse [27] and his group at NBS have studied reduced and doped $SrTiO_3$ and shown that a collective-electron, tight-binding model for the *d* electrons can account satisfactorily for

many details of the transport and magnetic properties that they have measured. With just a few charge carriers per cation, polaron theory should be applicable, and for narrow π^* bands a large-polaron $\rightleftarrows$ small-polaron, metallic $\rightleftarrows$ semiconducting transition might be anticipated from Holstein's theory. No such transition has been observed. In fact polaron theory is not required to interpret the data. Therefore we might conclude that the π^* band is relatively broad and that only large polarons are present. However, in $BaTiO_3$ there is a ferroelectric transition at $T_c = 120°C$, which indicates that the π and π^* bands are narrow enough for a narrow-band spontaneous distortion. To make contact with the discussion of section IIB, the π bands are filled and the π^* bands are empty in $BaTiO_3$. Below T_c the titanium displacements in the tetragonal phase are as shown in Fig. 14. In the basal plane the π^* bands are not transformed into "molecular" states, so that the basal-plane conductivity of slightly reduced or doped $BaTiO_3$ should be continuous through T_c. The arguments of section IIB can be easily extended to show that the titanium displacements in the lower temperature, orthorhombic and rhombohedral phases successively increase the energy gap in two and three dimensions.

It has been found [28] that $CaVO_3$ and $LaTiO_3$ are metallic and Pauli paramagnetic. Brixner [29] has reported similar properties for the system $Sr_{1-x}Ba_xMoO_3$. The rhombohedral perovskite $LaNiO_3$ contains trivalent nickel in a low-spin state and is metallic and Pauli paramagnetic [30], indicating the outer-electron configuration $t_{2g}^{*6}\sigma^{*1}$, and $LaRhO_3$ appears to be a narrow-gap semiconductor [31] corresponding to $t_{2g}^{*6}\sigma^{*0}$. $LaVO_3$ is a magnetic semiconductor [32] and $CaMnO_3$, $LaCoO_3$, $LaMnO_3$, and $LaFeO_3$ are magnetic insulators [33]. The fact that the system $La_{1-x}Ca_xMnO_3$ exhibits the magnetic order and structural properties characteristic

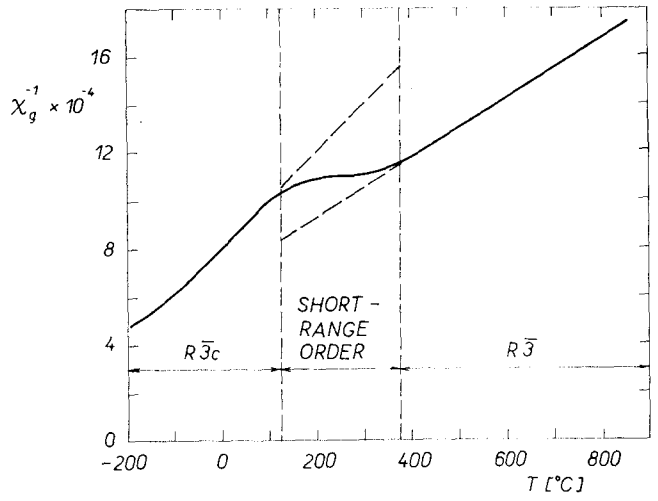

Fig. 15. Inverse magnetic susceptibility vs. temperature for $LaCoO_3$.

of superexchange and Jahn-Teller ordering at the Mn^{3+} ions [34] indicates that $\Delta_{cac}^{\sigma} < \Delta_c$ for Mn^{3+}. However, the relatively high conductivity below the Curie temperature of the ferromagnetic phase ($0{\cdot}2 < x < 0{\cdot}4$) suggests that $\Delta_{cac}^{\sigma} \to \Delta_c$ in this system, or that $\Delta_{cac}^{\sigma} > \Delta_c$ for $LaVO_3$, $CaMnO_3$, and $LaCrO_3$. $LaCoO_3$ demonstrates not only thermal equilibrium between high-spin and low-spin trivalent-cobalt ions, but also a first-order localized-electron $\rightleftarrows$ collective-electron transition at $T_t = 937°K$. Therefore it is shown as a bridge compound between regions II and III. The compound $SrFeO_3$ bridges regions I and II. It contains low-spin Fe^{4+} ions that appear to have three localized electrons of α-spin and one collective electron of β-spin ($t_\alpha^{*3}\pi_\beta^{*1}$)

[35]. $CaRuO_3$ and $SrRuO_3$ have only collective electrons (π^{*4}), but their magnetic properties indicate that they are a bridge between spontaneous band magnetism and Pauli paramagnetism, $SrRuO_3$ being ferromagnetic [36] and $CaRuO_3$ exhibiting a temperature-dependent susceptibility with a negative paramagnetic Curie temperature [36, 37].

The significant feature of Table 3 is the fact that region III is restricted to the high-spin ions having $S \geqq 2$. This clearly emphasizes the importance of intra-atomic exchange in stabilizing the localized-electron state. This effect was introduced into the empirical expression for R_c of Eq. (28) via the last term.

In the remainder of this paper, our discussion is confined to $LaCoO_3$ and to the grouping $SrFeO_3$, $SrRuO_3$, $CaRuO_3$ since the bridge compounds reveal information of interest about the nature of the transition in physical properties on going from a localized-electron to a collective-electron phase.

C. A First-Order Localized-Electron ⇄ Collective-Electron Transition

The inverse magnetic susceptibility vs. temperature curve for $LaCoO_3$ is shown in Fig. 15. It can be interpreted by a localized-electron model in which the energy difference between diamagnetic and paramagnetic trivalent cobalt is

$$\varepsilon_0 \equiv E_{3+} - E_{III} \leqq 0{\cdot}08 \text{ eV} \tag{29}$$

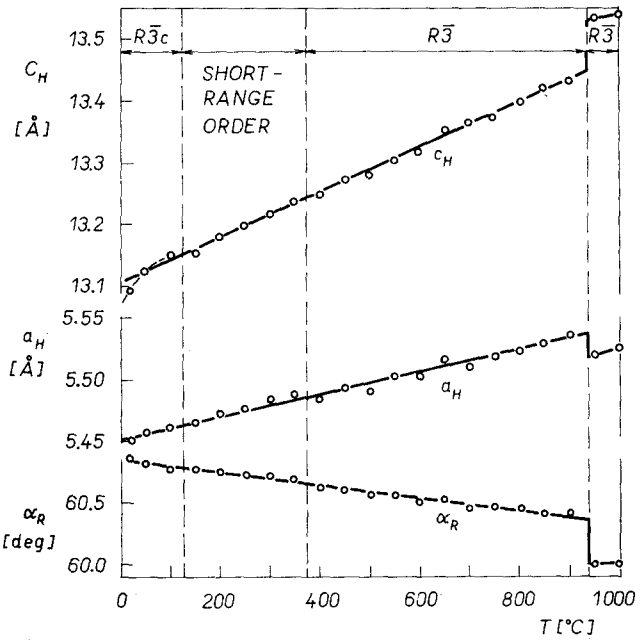

Fig. 16. Hexagonal-basis lattice parameters and rhombohedral angle vs. temperature for rhombohedral $LaCoO_3$.

where the low-spin ($S = 0$) $^1A_1$ ions, designated Co^{III}, are more stable than the high-spin ($S = 2$) $^5T_2$ ions, designated Co^{3+}. Low-spin ions have crystal-field splittings Δ_{cf} greater than intraatomic-exchange splittings Δ_{ex}. This interpretation is consistent with Table 3, since the crystal-field splitting $\Delta_{cf} \simeq 1$ eV $\gg \varepsilon_0$ and intraatomic exchange may localize the $3d$ electrons at a Co^{3+} ion ($t_{2g}^{*4}e_g^{*2}$) even though $\Delta_{cac}^{\sigma} > \Delta_c$ is anticipated for the Co^{III} ions ($t_{2g}^{*6}\sigma^{*0}$). In $LaRhO_3$, on the other hand, $\Delta_{cf} < \varepsilon_0$ and electrons are excited into a σ^* band rather than into the formation of high-spin ions. Although ions having $S = 2$ should have localized $3d$ electrons, according to Table 3, nevertheless in the presence of low-spin Co^{III} ions the average overlap integral $\langle \Delta_{cac}^{\sigma} \rangle$ may approach, or even exceed, the critical value Δ_c. Therefore the simultaneous existence of Co^{III} and Co^{3+} ions in $LaCoO_3$ immediately suggests the following possibilities: (1) High-spin and low-spin cobalt ions may order preferentially on alternate (111) cobalt planes, as suggested previously [38] for the system $La_{1-x}Sr_xCoO_3$, and (2) $LaCoO_3$ may have $\langle \Delta_{cac}^{\sigma} \rangle \approx \Delta_c$ and exhibit a first-order localized-electron $\rightleftarrows$ collective-electron transition.

Figures 16—19 show the results of precision x-ray measurements by Raccah [39] on a powder sample of the rhombohedral perovskite $LaCoO_3$. Thermogravimetric measurement revealed that samples lost oxygen if heated over 1050°C under hydrogen, so the measurements were

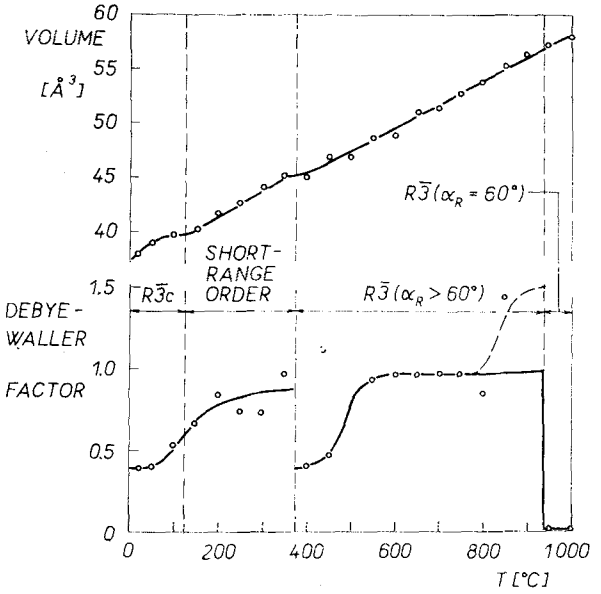

Fig. 17. Unit-cell volume and Debye-Waller factor vs. temperature for rhombohedral $LaCoO_3$.

limited to $T \leqq 1000$°C. Differential thermal analysis manifests an endothermic, first-order transition at $T_t = 937$°C and higher-order transitions in the interval $125 < T < 375$°C and at about 650°C.

The rhombohedral perovskite cell contains two molecules, as shown in Fig. 20. So long as the

transition-metal ion remains a center of inversion symmetry, three space groups are possible: $R\bar{3}c$, $R\bar{3}m$, and $R\bar{3}$. In the space group $R\bar{3}c$, the two cobalt ions are not distinguishable, and the close-packed, oxygen-lanthanum (111) planes remain equidistant from neighboring (111) cobalt planes. In the space groups $R\bar{3}m$ and $R\bar{3}$, the two cobalt-ion sites (Co_I and Co_{II}) per unit cell are not equivalent; the oxygen and lanthanum (111) planes, which coincide in $R\bar{3}c$ symmetry, are displaced independently along the c-axis. These displacements are in pairs toward Co_I planes and away from Co_{II} planes, so that the crystal-field splitting Δ_{cf} is larger at a Co_I site. The lanthanum displacements and the component of the oxygen displacements along [100] axes are shown schematically in Figs. 18, 19. Low-temperature neutron-diffraction studies [40] confirm that the symmetry is $R\bar{3}c$ from lowest temperatures to 125°C. In agreement with the second-order character of the transition between 125 and 375°C [41] the high-temperature symmetry is $R\bar{3}$. It is significant that the pseudocubic cell edge a_c and the volume remain constant, within experimental error, through the first-order phase change: only the rhombohedral angle α_R drops abruptly from 60·4 to 60·0° and the Debye-Waller factor drops by more than an order of magnitude.

Below 125°C, $LaCoO_3$ is a semiconductor with a conductivity given approximately by

$$\sigma = \sigma_0 \exp(-q/kT) \tag{30}$$

Above 125°C, the conductivity increases much more rapidly with increasing temperature, changing by over two orders of magnitude in the interval $125 < T < 650$°C. In the interval $650 < T < 937$°C the conductivity goes through a broad, flat maximum; it varies continuously through the transition temperature $T_t = 937$°C and decreases with increasing temperature, as in a metal, above 937°C.

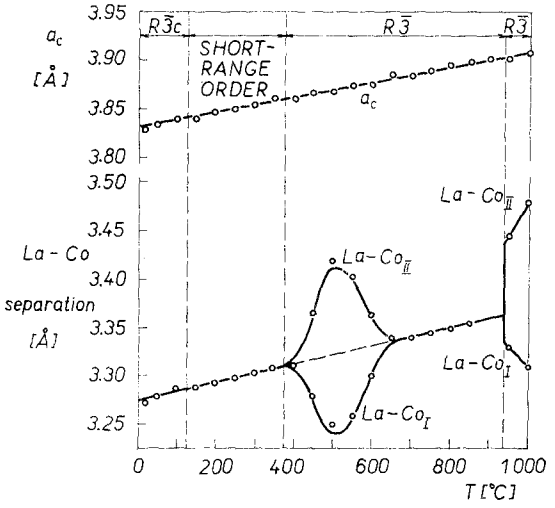

Fig. 18. Pseudocubic cell edge and La–Co_I, La–Co_{II} distances vs. temperature in $LaCoO_3$.

These changes in physical properties, including structure, can be interpreted with the model of Table 4 for each of the temperature intervals demarked by DTA and calorimetry:

(1) $-273 < T < 125$°C: High-spin Co^{3+} are thermally created, but randomly distributed, from the Co^{III}-ion ground-state matrix. This is possible because $\varepsilon_0 \leqq 0{\cdot}08$ eV $\ll \Delta_{cf} \sim 1$ eV. The conductivity has the form of Eq. (30) because the numbers of mobile charge carriers (electrons in orbitals of e_g symmetry and holes in orbitals of t_{2g} symmetry) are

Table 4

Model of Cobalt-Ion Configuration and *d*-electron Character in $LaCoO_3$ for Various Temperature Intervals

Co^{2+}, Co^{3+} = high-spin state and Co^{III}, Co^{IV} = low-spin state		
Temperature Interval	Dominant Cobalt-Ion Configuration	*d*-electrons
$-273 < T < 125$°C	Disordered Co^{3+} among majority Co^{III}	Localized
$125 \leqq T < 375$°C	Short-range order of Co^{3+} and Co^{III}	Localized
$375 \leqq T < 937$°C	Long-range order into Co_I and Co_{II}	Localized
$375 \leqq T \leqq 400$°C	(*a*) $Co_I = Co^{III}$; $Co_{II} = (1-x)\,Co^{3+} + xCo^{III}$	
$400 < T < 500$°C	(b) $Co_I = (1-y)\,Co^{III} + yCo^{2+}$; $Co_{II} = (1-x-y)\,Co^{3+} + xCo^{III} + yCo^{IV}$	
$500 \leqq T < 650$°C	(c) $Co_I = (1-y-z)\,Co^{III} + yCo^{2+} + zCo^{3+}$; $Co_{II} = (1-y-z)\,Co^{3+} + yCO^{IV} + zCo^{III}$	
$650 \leqq T < 937$°C	(d) $Co_I = (1-2\lambda-z)\,Co^{III} + \lambda(Co^{2+} + Co^{IV}) + zCo^{3+}$; $Co_{II} = (1-2\lambda-z)\,Co^{3+} + \lambda(Co^{IV} + Co^{2+}) + zCo^{III}$	
$937 < T \leqq 1000$°C	Long-range order: $Co_I(t_{2g}{}^{6-x}\sigma^{*y})$ $Co_{II}(t_{2g}{}^{4+x}\sigma^{*2-y})$; $x < y$	Collective

1. $x \to 0$ as increasing $T \to \sim 500$°C.
2. y increases from a small value at ~400°C to a maximum at ~500°C and decreases to a small value at ~600°C.
3. z increases from a small value at ~500°C to a relatively large value for $T \geqq 650$°C.
4. λ increases from a small value at ~650°C to a large value just below $T_t = 937$°C.

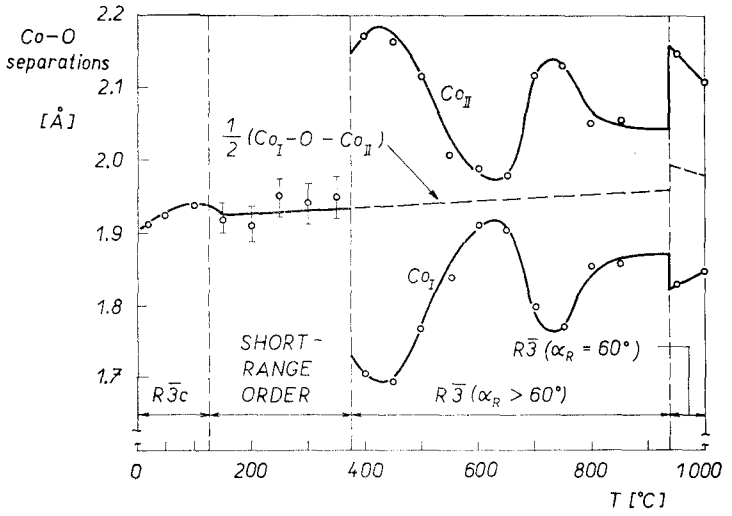

Fig. 19. Cobalt-oxygen separations vs. temperature for $LaCoO_3$.

(31) $$n = n_g = N\exp(-\varepsilon/2kT)\,; \quad p = p_{2g} = N\exp(-\varepsilon'/2kT)$$

where N is the number of cobalt ions per unit volume and

(32) $$\varepsilon = \varepsilon_0 + \varepsilon_g \quad \text{and} \quad \varepsilon' = \varepsilon_0 + \varepsilon_{2g}\,.$$

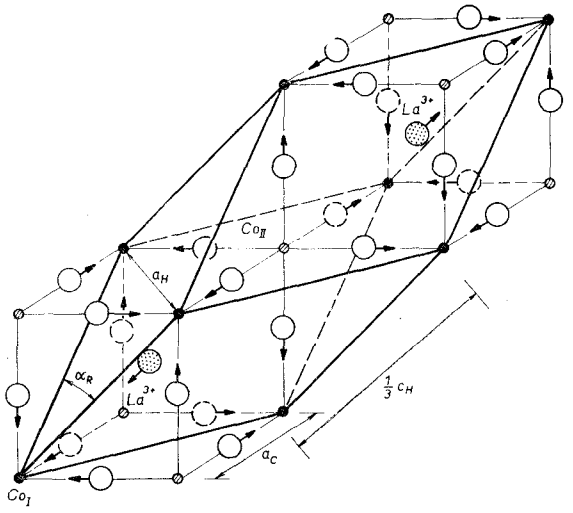

Fig. 20. Rhombohedral unit cell and definitions of lattice parameters for $LaCoO_3$. Directions of La^{3+}-ion and principal component of Co-ion displacements in symmetry $R\bar{3}$ are indicated by arrows.

Because the electrostatic energies ε_g, ε_{2g} required to create separated divalent and quadrivalent cobalt ions decrease with increasing overlap integral Δ_{cac}, where $\Delta^{\pi}_{cac} < \Delta^{\sigma}_{cac}$,

$$\varepsilon_g < \varepsilon_{2g} \quad \text{and} \quad n_g \geqq p_{2g} \tag{33}$$

even though the total number of holes and electrons (trapped plus mobile) are equal. The mobilities have the form of Eq. (16) with

$$\varepsilon_a \leqq 0{\cdot}05 \text{ eV} \tag{34}$$

(2) $125 \leqq T < 375$°C: The energy ε_0 is the splitting between the $^1A_1$ nondegenerate Co^{III} state and the threefold-degenerate $^5T_{2,1}$ state of Co^{3+}. The higher multiplets $J = 2,3$ of the $^5T_2$ state of Co^{3+} are separated from the $J = 1$ level by 2λ and 5λ, respectively, where $\lambda \approx \approx 400$ cm^{-1}. As the temperature increases toward $T_e = 420$°C, which is the solution of

$$\exp(\varepsilon_0/kT_e) = 3 + 5\exp(-2\lambda/kT_e) + 7\exp(-5\lambda/kT_e)\,.$$

As $kT \to \varepsilon_0$ with increasing temperature ($\varepsilon_0 = kT$ at $T \approx 200$°C), the populations of Co^{3+} and Co^{III} ions approach each other. Since the ions have different radii, elastic energy is conserved if only Co^{III} ions are near neighbors of every Co^{3+} ion. If the Co^{3+} population is large, this can only be realized by preferential ordering of Co^{3+} and Co^{III} ions on alternate (111) planes, as illustrated by sublattices Co_I and Co_{II} of Fig. 20. Note that this situation leads to the unusual occurrence of ordering at higher temperatures. Short-range order occurs in the interval $125 \leqq T < 375$°C. This ordering increases the number of minority atoms, Co^{3+}, thereby increasing the susceptibility and introducing the "plateau" in the $1/\chi_m$ vs. T curve of Fig. 15. An increase in the number of Co^{3+} ions also decreases the effective ε_0, thereby causing a sharp increase in the electrical conductivity. This effect is further enhanced by the fact that oxygen displacements towards Co^{III} ions away from Co^{3+} ions increase the overlap integrals $\langle\Delta^{\sigma}_{cac}\rangle$ and $\langle\Delta^{\pi}_{cac}\rangle$, so that ε_g and ε_{2g} also decrease.

(3) $375 \leqq T < 937$°C: The symmetry $R\bar{3}$ demonstrates preferential, long-range ordering of low-spin ions on Co_I sites, high-spin ions on Co_{II} sites. The parameter x of Table 4 for $T \leqq 500$°C is introduced because the Co^{3+}-ion population is still a minority population at the lower temperatures.

So long as the ions are primarily trivalent, the Co_I and Co_{II} sites carry approximately the same charge and there is no electrostatic field at the La^{3+} ions to displace them from the center of the pseudocube. However, as the conductivity increases, electrons and holes are transferred from the Co^{3+} ions, which are ordered preferentially on Co_{II} sites, to the Co^{III} ions on Co_I sites. Since Δ_{cf} is larger at a quadrivalent ion, smaller at a divalent ion, the Co^{IV} ions are low-spin and the Co^{2+} ions are high-spin whether on sublattice Co_I or Co_{II}. Therefore transfer of an electron, which is preferred because $\Delta^{\sigma}_{cac} > \Delta^{\pi}_{cac}$, is accompanied by transfer of an exciton from sublattice Co_{II} to sublattice Co_I. (Note that exciton transfer occurs wherever high-spin and low-spin ions are interchanged.) Charge transfer is not only indicated by the higher conductivity, but also by the displacements of the La^{3+} ions toward the Co_I sublattice, which is more negative than the Co_{II} sublattice. The decrease in oxygen-ion displacement results from the creation of high-spin Co^{3+} ions on sublattice Co_I and low-spin Co^{IV} ions on sublattice Co_{II}. As the temperature is further increased, electron transfer becomes saturated and hole transfer becomes relatively more important. Therefore σ continues to increase sharply to 650°C, but the La^{3+}-ion displacements disappear because hole and electron transfers become nearly equal. The fact that the oxygen-ion displacements continue to decrease to 650°C shows that the hole and electron transfers are coupled as excitons creating high-spin Co^{3+} on sublattice Co_I, low-spin Co^{III} on sublattice Co_{II}. It is only for $T > 650$°C that the hole and electron transfers are not correlated, and this allows some re-

storation of the ordering of low-spin ions on sublattice Co_I, high-spin ions on sublattice Co_{II}. This is reflected in the increase in anion displacements above 650°C.

(4) $937 < T \leqq 1000$°C: The cooperative displacements above 937°C of both the anions and the lanthanum ions manifest that long-range order is re-established. This is also reflected in the sharp drop of the Debye-Waller factor. The fact that band-electron correlations, in contrast to localized-electron correlations, are long-range indicates that long-range order has been re-established via the transformation of localized e_g orbitals into collective σ^*-band orbitals at $T_t = 937$°C. Since $\Delta^{\pi}_{cac} < \Delta^{\sigma}_{cac} \approx \Delta_c$, it follows that the orbitals of t_{2g} symmetry would remain localized, thereby still providing the distinction between two kinds of cobalt. With ideal long-range order, the Co_I sublattice contains cobalt ions with outer configuration $t_{2g}^{*6-x}\sigma^{*y}$ and the Co_{II} sublattice $t_{2g}^{*4+x}\sigma^{*2-y}$, where $x < y$, the fraction $\delta = x - y$ representing the transfer of electronic charge from sublattice Co_{II} to sublattice Co_I. This transfer of charge creates the electric field that displaces the La^{3+} ions.

(5) *The character of the transition at T_t*: The transition at $T_t = 937$°C is first-order and endothermic. Therefore the heat of transformation is

$$\Delta H = T_t \Delta S > 0 \tag{35}$$

where the entropy change at T_t is composed of configurational, vibrational, and electronic contributions:

$$\Delta S = \Delta S_{config} + \Delta S_{vib} + \Delta S_{el} > 0 \tag{36}$$

The fact that there is no change in the symmetry $R\bar{3}$ on passing through the transition indicates that $\Delta S_{config} \approx 0$. Since the large drop in Debye-Waller factor shows that $\Delta S_{vib} < 0$, it is concluded that

$$\Delta S_{el} > 0 \tag{37}$$

is the driving force for the first-order phase change. This conclusion is the strongest evidence for a localized-electron $\rightleftarrows$ collective-electron phase change at T_t, and it implies that there is a significant latent heat associated with the formation of collective electrons and their associated Fermi surface. This means that crystal-field theory, which rests on the assumption of localized electrons, and band theory, which describes a Fermi gas in a periodic potential, apply to two distinct thermodynamic states of the electrons.

Given this conclusion, it is at once of interest that there is no discontinuity in the electrical conductivity at T_t. In the model of Table 4, it is assumed that the numbers of holes and electrons are both saturated in the temperature interval $650 < T < 937$°C. So long as the width of the σ^*-band energies is $\Delta\varepsilon_b \leqq kT_t \approx 0{\cdot}1$ eV, all of the σ^*-band electrons are charge carriers. Therefore the number of charge carriers is unchanged by the transition from localized to collective electrons. This is unusual for a first-order transition, and it provides a rare opportunity to study the mobility change on passing through the transition. Since the conductivity is continuous, the mobility is continuous, which suggests that probably all physical properties that are in dependent of the existence of a Fermi surface are continuous through a loca-

lized-electron ⇄ collective-electron transition. However, the fact that conductivity measurements have only been made on sintered bars means that the rather surprising conclusion of a continuous mobility through T_t should be accepted with caution.

D. Spontaneous Band Magnetism

The compounds $SrFeO_3$, $SrRuO_3$, and $CaRuO_3$ each have four outer d electrons. $SrRuO_3$ and $CaRuO_3$ are definitely metallic, and polycrystalline samples of $SrFeO_3$ have a high ($\approx 10^3$ ohm^{-1} cm^{-1}), nearly temperature-independent conductivity that becomes semi-conducting in character only if $SrFeO_3$ is reduced [42]. $SrFeO_3$ is antiferromagnetic below 134°K, and the high-temperature susceptibility obeys a Curie-Weiss law, but with too large a Curie constant to be interpreted by crystal-field theory. It has been reported [42] to remain cubic to lowest temperatures. $SrRuO_3$, on the other hand, is ferromagnetic [36] below 154°K with a spontaneous moment of $0{\cdot}85\mu_B$/molecule in a field of 10KOe. Preliminary high-field data indicate that magnetic saturation has not been reached by 125 kgauss [43], whereas neutron-diffraction data show no canting of the rutheniumion spins and a spontaneous moment of $\leqq 1.0\mu_B$/molecule [44]. At high temperatures the inverse susceptibility vs. temperature curve obeys a Curie-Weiss law with an apparent $\mu_{eff} = 2{\cdot}6\mu_B$, which is high relative to the atomic moment measured at low temperatures, $CaRuO_3$ also obeys a Curie-Weiss law at high temperatures [36] and has an apparent $\mu_{eff} = 2{\cdot}98\mu_B$, which is somewhat larger than that found in $SrRuO_3$. More significant, the $1/\chi_m$ vs. T curve extrapolates to a negative intercept on the temperature axis, suggestive of antiferromagnetism.

These data, though preliminary, strongly support the following general scheme:

(1) There is a narrow range of bandwidths, or overlap integrals, over which spontaneous band magnetism may occur, as shown schematically in Fig. 7, and $SrRuO_3$ illustrates spontaneous band ferromagnetism of a π^* band that is two-thirds filled. The critical overlap integral Δ_c^f corresponds to Stoner's [45] maximum bandwidth for spontaneous ferromagnetism.

(2) The magnetic susceptibility of narrow-band electrons may be temperature-dependent, obeying a Curie-Weiss law at high temperatures, but the measured Curie constant increases rapidly from its localized-electron value with increasing bandwidth, becoming infinite (temperature-independent Pauli paramagnetism) only for bandwidths that are too large to support spontaneous band magnetism. This emphasizes the fact that measured Curie constants can only be interpreted by a localized-electron model, and such a model is only applicable to metals if broad conduction bands and localized orbitals are simultaneously present, as in the rare-earth metals. Where there are narrow conduction bands, as in metallic transition-metal alloys or compounds, the model is not applicable.

(3) Because intra-atomic exchange contracts the electron density about the atomic nuclei, overlap integrals for electrons in similar orbitals but different (α vs. β) spin states are

$$\Delta_\alpha < \Delta_\beta \quad \text{if} \quad S_\alpha > S_\beta \tag{38}$$

Further, it is necessary to distinguish between bonding orbitals and antibonding orbitals. Since bonding orbitals concentrate electronic charge into the metal-metal bonds, antibonding orbitals concentrate it away from the bonds. Therefore, in a three-dimensional array antibonding electrons are concentrated at the atomic sites like localized electrons. It follows that: (a) Bonding states tend to be split from antibonding states, making a bimodal density-of-states vs. energy profile. (b) The bonding orbitals occupy a broader band of energies than the antibonding orbitals, so that the overlap integrals for bonding vs. antibonding orbitals are

$$\Delta_b > \Delta_{ab} \tag{39}$$

This leads to three possible conditions for spontaneous band ferromagnetism:

$$\Delta_\alpha < \Delta_c < \Delta_\beta \tag{40}$$

$$\Delta_c < \Delta_b < \Delta_c^f \tag{41}$$

$$\Delta_c < \Delta_{ab} < \Delta_c^f < \Delta_b \tag{42}$$

Whether these conditions can be fulfilled depends upon the d-electron/atom ratio. There are three cases to be considered:

Half-filled band: Spontaneous magnetization of a half-filled band would create a filled α-spin band, an empty β-spin band. For a filled band, the localized-electron and band descriptions are equivalent. However, for localized electrons the energy can be reduced by introducing superexchange excited states, and this requires antiferromagnetic coupling of the localized electrons. Therefore the ferromagnetic state is not stable, and spontaneous ferromagnetism of a half-filled band is impossible. However, spontaneous band antiferromagnetism, which is described by a spin-density wave that introduces an energy discontinuity at the Fermi surface is possible.

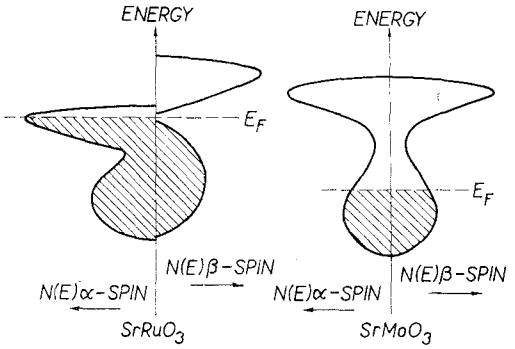

Fig. 21. Schematic density-of-states vs. energy profiles for π^* bands of ferromagnetic $SrRuO_3$ and paramagnetic $SrMoO_3$.

Less than quarter-filled band: Spontaneous magnetization of a quarter-filled band creates a half-filled α-spin band. Only bonding orbitals are occupied, and the ferromagnetic state may be competitive with a spin-density wave if Eq. (41) is satisfied. As the d-electron/atom ratio decreases, the wavelength of a stable spin-density wave increases (its stabilization energy decreases) and the ferromagnetic state is more probable.

More than three-quarters-filled band. Bonding orbitals are filled, and magnetization fills the α-spin orbitals by ordering the n_h antibonding-orbital holes per atom into β-spin orbitals. Ferromagnetism with a localized atomic moment of $n_h\mu_B$ can occur provided either Eq. (40), (41), or (42) is satisfied. Antiferromagnetism is not, in general, competitive.

More than half-filled, less than three-quarters-filled band. If Eq. (40) or (41) is satisfied, spontaneous magnetization creates localized α-spin electrons in the presence of collective β-spin electrons and a localized atomic moment of $n_h\mu_B$. Coupling of localized electrons via collective electrons is generally ferromagnetic, but a spiral-spin configuration may be competitive for critical values of n_h, corresponding to a small spiral wavelength to place an energy discontinuity at the Fermi surface.

However, if Eq. (42) is satisfied, then spontaneous magnetization only occurs among the antibonding electrons. In this case the magnetization per atom is reduced to $n_{ab}\mu_B$, where n_{ab} is the number of antibonding electrons per atom.

(4) Although the π^*-band states of metallic oxides with perovskite structure are antibonding with respect to the anionic sublattice, within the cationic sublattice they are both bonding and antibonding. Schematic density-of-states vs. energy curves for the π^* bands of $SrMoO_3$ and $SrRuO_3$ are shown schematically in Fig. 21. There are two π^* electrons and six π^* states (including spin) per $SrMoO_3$ molecule. Therefore the band is one-third filled, and the conditions for spontaneous ferromagnetism are not fulfilled. The π^* band of $SrRuO_3$, on the other hand, is two-thirds filled. Since it is ferromagnetic with a reduced atomic moment ($1\mu_B$ instead of $2\mu_B$), it is concluded that Eq. (42) applies. Note that there is just one antibonding π^* electron per molecule in $SrRuO_3$.

(5) Antiferromagnetic $SrFeO_3$ probably illustrates a case where Eq. (40) or (41) applies. With one β-spin electron per atom, a spin-density wave propagating along a [111] axis could be competitive with ferromagnetism.

(6) Although $CaRuO_3$ has a slightly smaller lattice parameter than $SrRuO_3$, the fact that Sr^{2+} is more ionic than Ca^{2+} means that Δ^{π}_{cac} is smaller in $CaRuO_3$ [46]. Apparently it represents spontaneous band antiferromagnetism, corresponding to Eq. (41) rather than Eq (42). These compounds require further study.

Received 18. 10. 1966.

References

[1] Goodenough J. B.: J. Phys. Soc. Japan *17* (1962), Suppl. B-I, 185.
[2] Verwey E. J. W., Haayman P. W., Romeijn F. C.: J. Chem. Phys. *15* (1947), 181.
[3] Vallet P., Raccah P. M.: Compt. Rend. Acad. Sci. (Paris) *258* (1964), 3679;
Carel C., Weigel D., Vallet P.: Compt. Rend. Acad. Sci. (Paris) *260* (1965), 4325.
[4] Goodenough J. B.: Bull. Soc. Chim. France *4* (1965), 1200.
[5] Goodenough J. B.: Description of Transition-Metal Compounds: Applications to Several Sulfides. Paper presented at Colloque International sur des Dérives Semi-métalliques, Université de Paris 1965.
[6] Bertaut E. F.: Bull. Soc. Fr. Minéral. et Cryst. *79* (1956), 276.
[7] Goodenough J. B.: J. Appl. Phys. *33* (1962), Suppl., 1197.
[8] Adler D.: Ph. D. Thesis. Physics Department, Harvard University, Cambridge, Mass., 1964.
[9] Pauling L.: The Nature of the Chemical Bond, 3rd ed. Cornell University Press, Ithaca (New York) 1960.
[10] Andersson S., Magnéli A.: Naturwiss. *43* (1956), 495; Acta chem. Scand. *11* (1950), 164.
[11] Gado P., Holmberg B., Magnéli A.: Acta chem. Scand. *19* (1965), 2010.
[12] Magnéli A.: Acta cryst. *6* (1953), 495.
[13] Sawyer J. O., Hyde B. G., Eyring L.: Bull. Soc. Chim. France *4* (1965), 1190; Hyde B. G., Bevan D. J. M., Eyring L.: Phil. Trans. Roy. Soc. (London) *A 259* (1966), 583.
[14] Magnéli A.: Nature *115* (1950), 356; Arkiv Kemi *1* (1950), 513.
[15] Overhauser A. W.: J. Phys. Chem. Solids *3* (1957), 311.
[16] Sato J., Toth R. S.: Phys. Rev. *124* (1961), 1833; *127* (1962), 469.
[17] Kaplan T. A.: Phys. Rev. *124* (1961), 329; J. Phys. Soc. Japan *17* (1962), Suppl. B-I, 3.
[18] Villain J.: J. Phys. Chem. Solids *11* (1959), 303.
[19] Yoshimori A.: J. Phys. Soc. Japan *14* (1959), 807.
[20] Fröhlich H., Sewell G. L.: Proc. Phys. Soc. (London) *74* (1959), 643.
[21] Holstein T.: Ann. of Phys. *8* (1959), 325, 343.
[22] Jonker G. H., van Houten S.: Halbleiterprobleme, Band VI (hrsg. von F. Sauter). Friedr. Vieweg und Sohn, Braunschweig 1961, 118.
[23] Jonker G. H.: J. Phys. Chem. Solids *9* (1959), 165.
[24] Shanks H. R., Sidles P. H., Danielson G. C.: Electrical Properties of the Tungsten Bronzes (Paper 22 in Nonstoichiometric Compounds, ed. by R. Ward; published as Advances in Chemistry Series 39). American Chemical Society, Washington D.C. 1963.
[25] Ferretti A., Rogers D. B., Goodenough J. B.: J. Phys. Chem. Solids *26* (1965), 2007.
[26] Feinleib J., Scouler W. T., Ferretti A.: Bull. Am. Phys. Soc. *11* (1966), 264.
[27] Frederikse H. P. R., Thurber W. R., Hosler W. R.: Phys. Rev. *134* (1964), A442.
[28] Johnston W. D., Sestrich D.: J. Inorg. Nucl. Chem. *20* (1961), 32;
Reuter B., Wollnik M.: Naturwiss. *17* (1963), 589;
Kern S., Rogers D. B. (unpublished research).
[29] Brixner L. M.: J. Inorg. Nucl. Chem. *14* (1960), 225.
[30] Goodenough J. B., Raccah P. M.: J. Appl. Phys. *36* (1965), Suppl., 1031.
[31] Raccah P. M. (personal communication).
[32] Rogers D. B., Ferretti A., Arnott R. J., Goodenough J. B.: J. Appl. Phys. *37* (1966), Suppl., 1431.
[33] Goodenough J. B.: Magnetism and the Chemical Bond. Interscience Publishers, New York—London 1963.
[34] Goodenough J. B.: Phys. Rev. *100* (1955), 564.
[35] Goodenough J. B.: J. Appl. Phys. *37* (1966), Suppl., 1415.
[36] Callaghan A., Moeller C. W., Ward R.: Inorg. Chem. *5* (1966), 1572.

[37] Longo J. M. (personal communication).
[38] Goodenough J. B.: J. Phys. Chem. Solids *6* (1958), 287.
[39] Raccah P. M., Goodenough J. B.: Phys. Rev. (to be published).
[40] Menyuk N., Dwight K., Raccah P. M.: J. Phys. Chem. Solids (to be published).
[41] Landau L. D., Lifshitz E. M.: Statistical Physics. Pergamon Press, London 1958, 439.
[42] MacChesney J. B., Sherwood R. C., Potter J. F.: J. Chem. Phys. *43* (1965), 1907.
[43] Foner S. (personal communication).
[44] Longo J. M., Raccah P. M. (personal communication).
]45] Stoner E. C.: Proc. Roy. Soc. (London) *A 165* (1938), 372; *A 119* (1939), 339; Phil. Mag. *25* (1938), 899.
[46] Goodenough J. B. (unpublished research).